Mean-squared displacement of a molecule moving in a glassy system

S.-H. Chong, W. Götze, and M. R. Mayr
Physik-Department, Technische Universität München, 85747 Garching, Germany
(Received 15 November 2000; published 20 June 2001)

The mean-squared displacement (MSD) of a hard sphere and of a dumbbell molecule consisting of two fused hard spheres immersed in a dense hard-sphere system is calculated within the mode-coupling theory for ideal liquid-glass transitions. It is proven that the velocity correlator, which is the second time derivative of the MSD, is the negative of a completely monotone function for times within the structural-relaxation regime. The MSD is found to exhibit a large time interval for structural relaxation prior to the onset of the α process, which cannot be described by the asymptotic formulas for the mode-coupling-theory–bifurcation dynamics. The α process for molecules with a large elongation is shown to exhibit an anomalously wide crossover interval between the end of the von Schweidler decay and the beginning of normal diffusion. The diffusivity of the molecule is predicted to vary nonmonotonically as a function of its elongation.

DOI: 10.1103/PhysRevE.64.011503 PACS number(s): 64.70.Pf, 61.25.Em, 61.20.Lc

I. INTRODUCTION

The mean-squared displacement $\delta r^2(t)$ (MSD) is a very transparent concept for the discussion of liquid dynamics [1]. For long times t, $\delta r^2(t)$ increases proportional to t and to the diffusion constant of the fluid. In an ideal solid, on the other hand, the long-time limit of $\delta r^2(t)$ is a finite number characterizing the square of the particle's localization length. Therefore, the long-time behavior of $\delta r^2(t)$ depends sensitively on control parameters such as density or temperature if the system is close to a liquid-glass transition point. The MSD is thus particularly well suited to study glass-transition precursors. It can be measured by incoherent inelastic-neutron-scattering experiments. However, $\delta r^2(t)$ has to be extracted as a small-wave-number limit of the intermediate scattering function [1], and this makes it very difficult to produce accurate data for large time intervals. Dynamic light-scattering spectroscopy and sample-preparation techniques for colloidal suspensions have improved greatly in recent years. It was demonstrated that very informative data for the MSD of hard-sphere colloids near the glass transition can be obtained [2], and promising results for this system have also been measured by direct-imaging techniques [3,4]. Molecular-dynamics simulations are well suited to get accurate data for the MSD for liquids near the glass transition. This was demonstrated for a binary Lennard-Jones mixture [5], for a liquid of diatomic molecules [6], for models for the van-der-Waals liquid orthoterphenyl [7,8], for a model for water [9], for a hard-sphere-colloid model [10], and for a model of silica [11]. In this paper, general features and some quantitative results for the evolution of the glassy dynamics as exhibited by the MSD will be considered within the mode-coupling theory (MCT) for ideal liquid-glass transitions.

The basic version of MCT is built on approximately derived closed equations of motion for the autocorrelation functions of density fluctuations. The essential input information is the equilibrium structure factors, which are anticipated to vary smoothly with the system's control parameters. At certain critical values for the latter, bifurcations occur from solutions for an ergodic liquid to ones for an amorphous nonergodic solid. Thus, MCT deals with a model for ideal liquid-glass transitions. The transition implies a novel dynamical scenario. Its features have been worked out by asymptotic solution of the equations. The leading-order asymptotic formulas establish universal results for the MCT transition, such as scaling laws, power-law divergencies for the time scales, and anomalous exponents for the spectra [12,13]. Many tests of the relevance of the MCT results for the explanation of the dynamics of glass-forming liquids have been performed, which are reviewed to some extent in Ref. [14]. Let us only mention here the recent analysis of data measured for propylene carbonate [15], studies by means of the optical Kerr effect [16,17], and the analysis of simulation data for a binary Lennard-Jones liquid [18] and for silica [19]. The outcome of these tests qualifies MCT as a candidate for a theory of glassy dynamics, and it seems justified to continue the preceding studies by exploring some of the implications for the MSD.

The intention of this paper is to identify further MCT results for future tests of this theory. The previous work on the hard-sphere system (HSS) [20–24] shall be continued by analyzing in detail the MSD for a tagged particle. The work on the MCT for molecular systems [25] will be extended by evaluating the MSD for the interaction sites of a symmetric dumbbell consisting of two fused hard spheres as well as for the molecule's center. The paper is structured as follows. In Sec. II, the equations to be solved are listed and the concepts to be used to discuss the results are described. Section III presents the results for the MSD and the analysis of its properties. In Sec. IV, the findings are summarized.

II. BASIC FORMULAS

A. Description of the system

In this section, the systems to be studied and the functions to be used for a description of their dynamics shall be defined. A system of N atoms of mass m distributed with density ρ is considered as solvent. The points in configuration space are specified by the particle positions $\vec{r}_\kappa$, $\kappa = 1,2,\ldots,N$. The basic variables for the description of the

structure are the density fluctuations with wave vector $\vec{q}$, $\rho_{\vec{q}}=\Sigma_\kappa \exp(i\vec{q}\cdot\vec{r}_\kappa)$. If $\langle\cdots\rangle$ denotes canonical averaging for temperature T, the structure factor is $S_q=\langle|\rho_{\vec{q}}|^2\rangle/N$, where $q=|\vec{q}|$ is the wave number. As the simplest example for a solute, a tagged atom of mass m_S and position $\vec{r}_S$ shall be considered. The distribution of the atom is described by the density fluctuation $\rho^S_{\vec{q}}=\exp(i\vec{q}\cdot\vec{r}_S)$. The solute-solvent interaction shall be characterized by the direct correlation function $c^S_q=\langle\rho^{S*}_{\vec{q}}\rho_{\vec{q}}\rangle/(\rho S_q)$. As a more complicated solute, a symmetric rigid diatomic molecule shall be chosen. Its position is specified by two interaction sites $(\vec{r}_A,\vec{r}_B)$, which have the same mass m_A. The position of the molecule can also be described by its center $\vec{r}_C=(\vec{r}_A+\vec{r}_B)/2$ and the unit vector $\vec{e}=(\vec{r}_A-\vec{r}_B)/L$, where $L=|\vec{r}_A-\vec{r}_B|$. The configuration variables for the molecule can be built with the two density fluctuations $\rho^a_{\vec{q}}=\exp(i\vec{q}\cdot\vec{r}_a)$; $a=A$, B. Equivalently, one can use the number fluctuations $\rho^N_{\vec{q}}=(\rho^A_{\vec{q}}+\rho^B_{\vec{q}})/\sqrt{2}$ and the ''charge'' fluctuations $\rho^Z_{\vec{q}}=(\rho^A_{\vec{q}}-\rho^B_{\vec{q}})/\sqrt{2}$. The solute-solvent interaction can be characterized by the direct interaction-site-solvent correlations $c^A_q=c^B_q=\langle\rho^{A*}_{\vec{q}}\rho_{\vec{q}}\rangle/[\rho S_q w^N_q]$ [26]. Here $w^{N,Z}_q=1\pm\sin(qL)/qL$ denote the intramolecular structure factors.

Three kinds of mean-squared displacement functions of time t shall be discussed, $\delta r^2_x(t)=\langle[\vec{r}_x(t)-\vec{r}_x(0)]^2\rangle$. Here and in the following, the label $x=S$, C, and A refers to the position of a tagged particle, of the center of the molecule, and of the atomic center in the molecule, respectively. It will be more convenient to use the following abbreviation:

$$\Delta_x(t)=\tfrac{1}{6}\,\delta r^2_x(t),\quad x=S,C,A. \tag{1}$$

The MSD of the molecule's constituents can be decomposed into one contribution due to translation of the center and one due to reorientation of the axis [25],

$$\Delta_A(t)=\Delta_C(t)+\tfrac{1}{12}\,L^2\,[1-C_1(t)], \tag{2}$$

where

$$C_1(t)=\langle\vec{e}(t)\cdot\vec{e}\,\rangle \tag{3}$$

is the dipole correlator. The time derivatives of the MSD provide the velocity-autocorrelation function [1]. Let us consider the one for the velocity $\vec{v}_S(t)$ of the tagged particle only, $K_S(t)=\langle\vec{v}_S(t)\cdot\vec{v}_S\rangle$, where

$$\partial_t^2\Delta_S(t)=\tfrac{1}{3}\,K_S(t). \tag{4}$$

The nontrivial time dependence of $\vec{r}_x(t)-\vec{r}_x(0)$ comes about since the forces on the solute fluctuate in time, and this is caused by the density fluctuations of the solvent and by the fluctuations of the probability density of the solute constituents. These quantities are described by the density correlator $\phi_q(t)=\langle\rho_{\vec{q}}(t)^*\rho_{\vec{q}}\rangle/\langle|\rho_{\vec{q}}|^2\rangle$ of the solvent, by the tagged-particle-density correlator $\phi^S_q(t)=\langle\rho^S_{\vec{q}}(t)^*\rho^S_{\vec{q}}\rangle$, and by the molecule's correlators $\phi^{N,Z}_q(t)=\langle\rho^{N,Z}_{\vec{q}}(t)^*\rho^{N,Z}_{\vec{q}}\rangle/w^{N,Z}_q$. These correlators also determine the desired functions, since [1,25]

$$\phi^S_q(t)=1-q^2\,\Delta_S(t)+O(q^4), \tag{5a}$$

$$\phi^N_q(t)=1-q^2\,\Delta_C(t)+O(q^4), \tag{5b}$$

$$\phi^Z_q(t)=C_1(t)+O(q^2). \tag{5c}$$

B. MCT approximations

In this section, those equations shall be listed that have to be solved numerically. Within the Zwanzig-Mori theory, an exact equation of motion can be formulated for the density correlator: $\partial_t^2\phi_q(t)+\Omega_q^2\,\phi_q(t)+\int_0^t dt'\,M_q(t-t')\,\partial_{t'}\phi_q(t')=0$. Here $\Omega_q^2=v^2q^2/S_q$ with v denoting the thermal velocity specifies a characteristic frequency Ω_q, and $M_q(t)$ denotes a fluctuating-force correlator called the relaxation kernel [1]. Within MCT, the kernel is split into a regular part $M^{\rm reg}_q(t)$ dealing with normal-liquid effects and a mode-coupling kernel $\Omega_q^2 m_q(t)$ describing the cage effect. If one introduces an operator $\mathcal{R}$ for the regular dynamics by $\mathcal{R}\phi_q(t)=[\partial_t^2\phi_q(t)+\int_0^t dt'\,M^{\rm reg}_q(t-t')\,\partial_{t'}\phi_q(t')]/\Omega_q^2$, one can write

$$\mathcal{R}\phi_q(t)+\phi_q(t)+\int_0^t dt'\,m_q(t-t')\,\partial_{t'}\phi_q(t')=0. \tag{6}$$

The crucial step in the derivation is the application of Kawasaki's factorization approximations to express the kernel $m_q(t)$ as the mode-coupling functional $\mathcal{F}_q$ of the correlators,

$$m_q(t)=\mathcal{F}_q[\phi_k(t)], \tag{7a}$$

$$\mathcal{F}_q[\tilde{f}_k]=\frac{1}{2(2\pi)^3}\int d\vec{k}\,V(\vec{q};\vec{k},\vec{p}\,)\,\tilde{f}_k\tilde{f}_p\,. \tag{7b}$$

Here $\vec{p}$ is short for $\vec{q}-\vec{k}$. The coefficients $V(\vec{q};\vec{k},\vec{p}\,)$ are given in terms of the structure factor [27].

None of the MCT results for structural relaxations, in particular none of the universal results to be cited in Sec. II C, depend on the model for $M^{\rm reg}_q(t)$. The details of the kernel merely influence the value of some time scale to be denoted below as t_0. But the kernel $M^{\rm reg}_q(t)$ shall be specified in order to have controllable quantitative results for all times. Specifically, a model with $M^{\rm reg}_q(t)\equiv 0$ shall be chosen. The operator $\mathcal{R}$ shall be complemented by an index H indicating that a Hamiltonian dynamics is considered for the short-time motion,

$$\mathcal{R}^H\phi_q(t)=\partial_t^2\phi_q(t)\,/\,\Omega_q^2\,. \tag{8a}$$

This model overemphasizes oscillation features. A more realistic model would include at least some friction term as it is caused for low-frequency phenomena by binary collision events. But no detailed proposals for the treatment of such effects have been made so far within MCT. Some results also will be presented for a simplified colloid model. Here, the

inertia term from Eq. (8a) is neglected and the regular term is chosen as a q-independent white-noise kernel. It is explained in more detail in Appendix A that this model corresponds to the conventional treatment of colloids by coarse-graining the time over intervals of the duration of collisions of the solvent molecules with the mesoscopic colloid particles. As a result, the short-time motion is treated by a Brownian dynamics,

$$\mathcal{R}^{\mathrm{B}}\phi_q(t)=\tau_q\,\partial_t\phi_q(t). \tag{8b}$$

Here $\tau_q=S_q/(D_0q^2)$ with D_0 denoting the single-particle diffusion constant.

Equations (6) and (8) hold analogously for the solute correlators $\phi_q^x(t)$, $x=S$, N, and Z. One gets $(\Omega_q^S)^2=v_S^2q^2$ with v_S denoting the tagged particle thermal velocity. The relaxation time for the Brownian motion is $\tau_q^S=1/(D_0^Sq^2)$ with D_0^S denoting the tagged particle short-time diffusivity. The more involved expressions for the characteristic frequencies $\Omega_q^{N,Z}$ can be found in Ref. [25]. Brownian dynamics shall not be considered for the dumbbell molecule. The fluctuating-force kernels are functionals of the correlators $\phi_q^x(t)$ and $\phi_q(t)$:

$$m_q^x(t)=\mathcal{F}_q^x[\,\phi_k^x(t),\phi_p(t)\,], \tag{9a}$$

$$\mathcal{F}_q^x[\tilde f_k^x,\tilde f_p]=\frac{1}{(2\pi)^3}\int d\vec k\,V^x(\vec q;\vec k,\vec p\,)\,\tilde f_k^x\tilde f_p,\quad x=S,N,Z. \tag{9b}$$

Again, $\vec p$ is short for $\vec q-\vec k$ and the coefficients $V^x(\vec q;\vec k,\vec p)$ are given by S_q and the direct correlation functions [25,27]. It is cumbersome to calculate the required $q\to0$ limits in Eqs. (5) numerically from numerical solutions for $\phi_q^x(t)$. It is more adequate to carry out the limit analytically in the equations of motion for $\phi_q^x(t)$ so that one gets equations of motion for the desired functions. The nontrivial parts of these equations are convolution integrals defined with the $q\to0$ limits of the kernels $m_q^x(t)$. One gets for the dipole correlator,

$$\partial_t^2C_1(t)+2v_R^2\,C_1(t)+2v_R^2\int_0^t dt'\,m_Z(t-t')\,\partial_{t'}C_1(t')=0, \tag{10}$$

where v_R is the thermal angular velocity of the molecule [25]. From the equation for $\phi_q^S(t)$, one gets a Zwanzig-Mori equation for the velocity correlator [12],

$$\partial_tK_S(t)+v_S^2\int_0^t dt'\,m_S(t-t')\,K_S(t')=0. \tag{11}$$

Integrating twice over t, one gets, with the aid of Eq. (4) and the initial conditions $\Delta_S(0)=0$ and $\partial_t\Delta_S(0)=0$,

$$H:\ \ \partial_t\Delta_S(t)-v_S^2\,t+v_S^2\int_0^t dt'\,m_S(t-t')\,\Delta_S(t')=0. \tag{12a}$$

The corresponding equation for Brownian short-time dynamics [23] is derived in Appendix A:

$$B:\ \ \Delta_S(t)-D_0^S\,t+D_0^S\int_0^t dt'\,m_S(t-t')\,\Delta_S(t')=0. \tag{12b}$$

The same procedure leads to the equation of motion for the MSD of the center:

$$H:\ \ \partial_t\Delta_C(t)-v_T^2\,t+v_T^2\int_0^t dt'\,m_N(t-t')\,\Delta_C(t')=0, \tag{13}$$

where the kernel is denoted by $m_N(t)$ and v_T is the thermal velocity for the molecule's translation [25]. The problem of the molecule's dynamics reduces to that of a tagged atom with $m_S=2m_A$, if the limit $L\to0$ is considered.

The kernels in the preceding Eqs. (10)–(13) are given by mode-coupling functionals,

$$m_x(t)=\mathcal{F}^x[\,\phi_k^x(t),\phi_p(t)\,], \tag{14a}$$

$$\mathcal{F}^x[\tilde f_k^x,\tilde f_p]=\frac{1}{6\pi^2}\int_0^\infty dk\,k^4\,\rho S_k\,v^x(k)\,\tilde f_k^x\tilde f_k,\quad x=S,N,Z. \tag{14b}$$

Here $v^S(k)=(c_k^S)^2$ [27], $v^N(k)=2(c_k^A)^2w_k^N$, and $v^Z(k)=(L^2/6)(c_k^A)^2w_k^Z$ [25]. A fluctuating force with vanishing wave vector can couple to density fluctuations of the solvent for all wave vectors $\vec k$ provided the atom or molecule can absorb the recoil with wave vector $-\vec k$. Therefore, one needs the superposition of density correlators $\phi_k(t)$ and $\phi_k^x(t)$ for all wave numbers k for the calculation of the kernels $m_x(t)$.

C. Universal results

Universal properties of the MCT–glass-transition scenario are formulated by the leading-order asymptotic expressions for the long-time dynamics for states near the transition points. This paper focuses on features beyond the universal ones, but the universal formulas shall be used as reference. In this section, those formulas [12] shall be compiled that are needed in Sec. III for the description of the results.

The equilibrium structure of the system may depend on, say, n control parameters, which can be combined to a control-parameter vector V. A separation parameter $\sigma(V)$, a smooth function of V, can be defined with the aid of the mode-coupling functional $\mathcal{F}_q$. For states with control parameters V such that $\sigma<0$, correlation functions decay to zero: $\phi_q(t\to\infty)=0$. But for states with $\sigma>0$, density fluctuations exhibit spontaneous arrest: $\phi_q(t\to\infty)=f_q>0$. The Debye-Waller factor f_q is to be evaluated from the mode-coupling functional $\mathcal{F}_q$ in Eqs. (7) via the equation $f_q/(1-f_q)=\mathcal{F}_q[f_k]$ [27]. The set of critical points V^c, defined by $\sigma(V^c)=0$, separates liquid states from glass states. This result holds for all correlators $\phi_A(t)=\langle A(t)^*A\rangle/\langle|A|^2\rangle$ of variables A coupling to density fluctuations. While $\phi_A(t\to\infty)$ vanishes for the liquid, generically, the limit $f_A=\phi_A(t\to\infty)$ is positive for the glass. If A refers to $\rho_{\vec q}$, $\rho_{\vec q}^S$, or $\vec e$, f_A denotes the Debye-Waller factor f_q, the Lamb-

Mössbauer factor f_q^S, or the Edwards-Anderson parameter f_1, respectively, of the glass. Crossing the transition points, the long-time limit changes discontinuously from zero to the critical value f_A^c. For the variation of f_A upon approaching the transition from the glass side, one gets for small σ in leading order

$$f_A = f_A^c + h_A \sqrt{|\sigma|} / \sqrt{1-\lambda}. \tag{15}$$

Here h_A is called the critical amplitude for variable A. Every point V^c is characterized by a number λ, $0<\lambda<1$, which is called the exponent parameter. The significance of λ is explained below in connection with Eqs. (16)–(18). It is a matter of convention not to incorporate $\sqrt{1-\lambda}$ in the amplitude h_A, in order to simplify some of the following formulas. The quantities f_A^c, h_A, and λ are calculated from $\mathcal{F}_q$. They are equilibrium quantities that are the same for Hamiltonian and Brownian dynamics.

The parameter λ determines an anomalous exponent a, $0<a<\frac{1}{2}$, which is called the critical exponent. The equation $\Gamma(1-a)^2/\Gamma(1-2a)=\lambda$ holds, where Γ denotes the gamma function. The long-time decay at the critical point is given, up to corrections of order t^{-2a}, by the power law

$$\phi_A(t) = f_A^c + h_A (t_0/t)^a, \quad \sigma = 0, \quad t/t_0 \gg 1. \tag{16}$$

The A-independent time t_0 is the relevant microscopic scale for the bifurcation dynamics. It depends on all details of the transient dynamics as well as on the mode-coupling functionals for parameters at the transition point.

The first scaling law of MCT deals with the dynamics for small σ in a time interval where $\eta = \phi_A(t) - f_A^c$ is small. In a leading expansion for $\sigma \to 0$ and $\eta \to 0$, one gets

$$\phi_A(t) = f_A + h_A G(t), \tag{17a}$$

$$G(t) = \sqrt{|\sigma|}\, g_\pm(t/t_\sigma), \quad \sigma \gtrless 0, \tag{17b}$$

$$t_\sigma = t_0 / |\sigma|^\delta, \quad \delta = 1/2a. \tag{17c}$$

The functions $g_\pm(\hat{t})$ are determined by λ. Thus, the control-parameter dependence of the dynamics is determined by the correlation scale $\sqrt{|\sigma|}$ and by the first critical time scale t_σ. One gets $g_\pm(\hat{t} \to 0) = 1/\hat{t}^a$, so that Eq. (16) is reproduced for fixed large t if σ tends to zero. Since $g_+(\hat{t} \to \infty) = 1/\sqrt{1-\lambda}$, also Eq. (15) is reproduced.

The equation $g_-(\hat{t} \to \infty) = -B\hat{t}^b + O(1/\hat{t}^b)$ holds. The anomalous exponent b, $0<b\leqslant 1$, which is called the von Schweidler exponent, is to be calculated from the equation $\Gamma(1+b)^2/\Gamma(1+2b)=\lambda$. The constant B is of order unity. Substituting this result into Eqs. (17), one gets von Schweidler's law for the decay of the liquid correlator below the plateau f_A^c,

$$\phi_A(t) = f_A^c - h_A (t/t'_\sigma)^b, \quad t_\sigma \ll t, \quad \sigma \to -0. \tag{18a}$$

The control-parameter dependence is described by the second critical time scale,

$$t'_\sigma = t_0\, B^{-1/b} / |\sigma|^\gamma, \quad \gamma = (1/2a) + (1/2b). \tag{18b}$$

Following the terminology of the glass-transition literature, the decay of $\phi_A(t)$ below the plateau f_A^c is called the α process. For this process, the second scaling law of MCT in leading order for $\sigma \to -0$ holds:

$$\phi_A(t) = \tilde{\phi}_A(\tilde{t}), \quad \tilde{t} = t/t'_\sigma, \quad t_\sigma \ll t. \tag{19}$$

The control-parameter-independent shape function $\tilde{\phi}_A(\tilde{t})$ is to be evaluated from the mode-coupling functionals at the critical points V^c. The differences of the dynamics as they are caused by different models for the short-time dynamics merely enter via differences in the scale t_0. For short rescaled times $\tilde{t}$, one gets $\tilde{\phi}_A(\tilde{t}) = f_A^c - h_A\tilde{t}^b + h'_A\tilde{t}^{2b} + \cdots$, so that Eq. (18a) is reproduced. The ranges of applicability of the first and the second scaling laws overlap; both scaling laws imply von Schweidler's law for $t_\sigma \ll t \ll t'_\sigma$.

Suppose the system is driven through the transition point V^c by smooth variation of some parameters θ such as the temperature, the density, or, for a colloid, the salt concentration of the solvent. Let θ^c denote the value where $V(\theta^c) = V^c$. Then one can write for σ, in leading order for small $(\theta - \theta^c)$, the expression $\sigma = C_\theta(\theta - \theta^c)/\theta^c$. The constant C_θ depends on the choice of θ and connects the distance parameter $\epsilon = (\theta - \theta^c)/\theta^c$ with the relevant separation parameter σ.

D. The model

Hard spheres of diameter d shall be used as a model for the solvent atoms. For this case, all equilibrium quantities are specified by the packing fraction $\varphi = \pi\rho d^3/6$. The MCT model for the hard-sphere system (HSS) will be defined by two further technical assumptions. First, the structure factor S_q and the direct correlation function c_q are evaluated within the Percus-Yevick theory [1]. Second, the wave numbers are discretized to 100 equally spaced values $qd = 0.2, 0.6, 1.0, \ldots, 39.8$. The details of the transformation of the functional in Eq. (7b) to a polynomial in the 100 variables $\phi_q(t)$ can be found in Ref. [22]. Representative solutions are shown in Refs. [24] and [28] for the Hamiltonian dynamics and in Ref. [22] for the Brownian dynamics. There is a liquid-glass transition at the critical packing fraction $\varphi_c \approx 0.516$ [22,27]. For the exponent parameter, one gets $\lambda = 0.735$, and this implies

$$a = 0.312, \quad b = 0.583, \quad B = 0.836, \quad \delta = 1.60, \quad \gamma = 2.46. \tag{20a}$$

For the separation parameter σ, one gets in leading order

$$\sigma = 1.54\,\epsilon, \quad \epsilon = (\varphi - \varphi_c)/\varphi_c. \tag{20b}$$

The microscopic time scales t_0 for Hamiltonian dynamics [28] and Brownian dynamics [22], respectively, are

$$t_0^H = 0.0236\,(d/v), \quad t_0^B = 0.002\,65\, d^2/D_0. \tag{21}$$

As an atomic solute, a tagged particle of the solvent shall be considered, i.e., $m_S=m$, and c_q^S is identical with the direct correlation function c_q of the HSS. As a molecular solute, a symmetric dumbbell of two fused hard spheres of diameter d and mass $m_A=m$ shall be chosen. The elongation $\zeta=L/d$ shall be used as the control parameter of the solute. The wave numbers are chosen discrete as above. The direct correlation function c_q^A is expressed as series of contributions $c_\ell(q), \ell=0,1,\ldots,$ obtained by expanding the molecule-solvent correlations in spherical harmonics [25]. The sum over ℓ is truncated at $\ell_{co}=8$. The $c_\ell(q)$ are evaluated with the Percus-Yevick theory [29]. Representative results for the molecule's correlators $\phi_q^N(t)$, $\phi_q^Z(t)$, and $C_1(t)$ are shown in Ref. [25], and those for $\phi_q^S(t)$ for the Brownian dynamics are in Ref. [23].

The figures to be discussed below and the numbers to be mentioned are evaluated for the above-specified model as follows. First, for a representative set of packing fractions, Eqs. (6) and (7) are solved for the density correlators $\phi_q(t)$, both for Hamiltonian as well as Brownian dynamics. These correlators are used to define the kernels in Eqs. (9), so that, as a second step, the tagged particle correlators $\phi_q^S(t)$ could be evaluated, also for both examples for the short-time dynamics. Furthermore, for every φ, the equations for the molecule's correlators $\phi_q^{N,Z}(t)$ are solved for 10 values for the elongation ζ. These results are substituted into Eqs. (14) for the kernels $m_x(t)$ so that, as a last step, Eqs. (10)–(13) for the desired functions $\Delta_x(t)$, $C_1(t)$, and $K_S(t)$ can be solved.

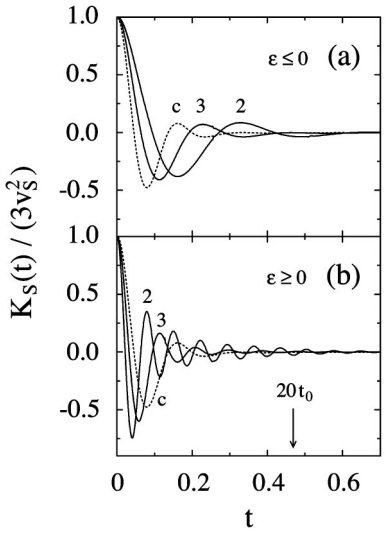

FIG. 1. Normalized velocity-correlation functions $K_S(t)/(3v_S^2)$ for a tagged particle of the hard-sphere system (HSS). The dotted lines with label c refer to the critical packing fraction $\varphi_c\approx 0.516$. The full lines with labels $n=2$ and 3 are calculated for distance parameters $\epsilon=(\varphi-\varphi_c)/\varphi_c=\mp 10^{-n/3}$ for the liquid ($\epsilon<0$) and for the glass ($\epsilon>0$), respectively. Here and in some of the following figures, an arrow marks the time $20t_0$, where $t_0=t_0^H=0.0236(d/v)$ is the time scale from Eqs. (16) and (21) for the critical decay. The units of length and of time are chosen here and in the following figures so that the particle diameter d and the thermal velocities $v=v_S$ are unity.

III. RESULTS

A. The diffusion-localization transition

If a tagged particle would experience a mere Newtonian friction force, the velocity correlations would decay exponentially, $K_S(t)\propto\exp[-(t/\tau)]$. The cage effect in dense liquids manifests itself by a qualitatively different behavior, namely by oscillatory variations with a decay of $K_S(t)$ to negative values [1]. Figure 1(a) demonstrates this phenomenon. With increasing density, the crossover time to negative values shortens and the damping of the oscillations increases. A Green-Kubo formula relates the particle diffusivity D_S to the zero-frequency velocity spectrum: $D_S=(1/3)\int_0^\infty dt\, K_S(t)$ [1]. Negative contributions to $K_S(t)$ reduce the diffusivity with increasing φ. From Eq. (11), one gets D_S as the inverse of the zero-frequency spectrum of the relaxation kernel [12]: $D_S=1/\int_0^\infty dt\, m_S(t)$. From Eqs. (12), one obtains for the long-time asymptote of the MSD $\lim_{t\to\infty}\Delta_S(t)/t=D_S$ [1].

For glass states, density fluctuations arrest for long times: $\phi_q^S(t\to\infty)=f_q^S>0$. The Lamb-Mössbauer factor f_q^S is to be evaluated from the mode-coupling functional $\mathcal{F}_q^S$ in Eqs. (9) via the equation $f_q^S/(1-f_q^S)=\mathcal{F}_q^S[f_k^S,f_p]$ [27]. It approaches unity for q tending to zero. A localization length r_S can be introduced to characterize the width of the f_q^S-versus-q curve: $f_q^S=1-(qr_S)^2+O(q^4)$. From Eq. (5a), one gets for the MSD $\lim_{t\to\infty}\Delta_S(t)=r_S^2$. Using Eqs. (12), one can express r_S^2 as the inverse of the long-time limit of the relaxation kernel [12]: $r_S^2=1/m_S(t\to\infty)=1/\mathcal{F}^S[f_k^S,f_p]$. If the density increases, the localization length r_S decreases. As a result, the frequency of the oscillations of the particles in their frozen cages increases, as is shown in Fig. 1(b). But, in contrast to what is found for liquid states, the damping of the oscillations decreases upon compression. This reflects the formation of anomalous oscillation peaks in the density-fluctuation spectra, which have properties of the so-called boson peaks of liquids and glasses [24].

The ideal liquid-glass transition implies a transition from a regime with particle diffusion for $\varphi<\varphi_c$ to one with particle localization for $\varphi\geqslant\varphi_c$. The former is characterized by $D_S>0$ and $1/r_S=0$ and the latter by $D_S=0$ and $1/r_S>0$. The subtleties of the glass-transition dynamics occur outside the transient regime. They can be discussed best on logarithmic scales as in Fig. 2. For very short times, say $t\leqslant t_0$, interaction effects are unimportant and $\lim_{t\to 0}\Delta_S(t)/t^2=v_S^2/2$ reflects ballistic motion. For times larger than t_0, the cage effect leads to a suppression of $\Delta_S(t)$ below the short-time asymptote. For such large times that $\delta r_S^2(t)/d^2$ reaches unity, the MSD approaches the diffusion asymptote, $\Delta_S(t)\approx D_S t$, as is shown by the dotted straight lines drawn for the curves with labels $n=1$ and $n=9$. Upon increasing φ towards φ_c, the diffusivity decreases towards zero. Figure 3 shows that the power law $D_S^{1/\gamma}\propto|\epsilon|$ for $|\epsilon|<0.1$ holds.

The lowest line in Fig. 2 deals with the same glass state $\varphi=1.1\varphi_c$, which was considered in Fig. 1(b) for the label $n=3$. For this density, there is no obvious glassy dynamics. Rather, $\Delta_S(t)$ has approached its long-time limit r_S^2 after the oscillations have disappeared for $t\approx 1$. Decreasing φ to-

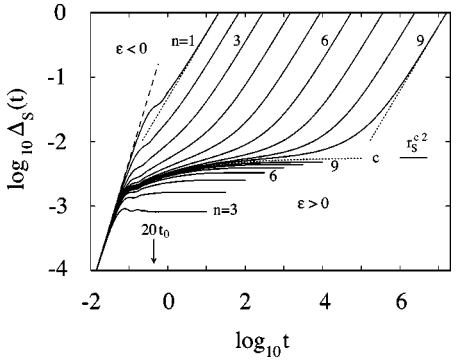

FIG. 2. Double logarithmic presentation of $\Delta_S(t)=\delta r_S^2(t)/6$ for the mean-squared displacement (MSD) $\delta r_S^2(t)$ for a tagged particle of the HSS. The dotted line with label *c* refers to the critical packing fraction φ_c and the full ones to $\epsilon=\pm 10^{-n/3}$. The straight dashed line with slope 2 exhibits the ballistic asymptote $(v_S t)^2/2$. The straight dotted lines with slope 1 exhibit the long-time asymptotes $D_S t$ of the two liquid curves for $n=1$ and 9. The horizontal line marks the square of the localization length at $\varphi=\varphi_c$: $r_S^{c\,2}=0.005\,57\,d^2$.

wards φ_c, the softening of the glass manifests itself by an increase of the localization length r_S. At the transition point $\varphi=\varphi_c$, the critical value $r_S^c=0.0746\,d$ is reached. This upper limit for r_S is consistent with Lindemann's melting criterion [27]. Using Eq. (15) for f_q and f_q^S and substituting these formulas into $\mathcal{F}^S[f_k^S,f_p]$, it follows that the glass instability at φ_c causes a $\sqrt{\sigma}$ anomaly for the localization length,

$$r_S^2=r_S^{c\,2}-h_S\sqrt{\sigma}/\sqrt{1-\lambda}+O(\sigma), \tag{22}$$

where $r_S^{c\,2}=0.005\,57\,d^2$ and $h_S=0.0116\,d^2$. Figure 3 demonstrates that the leading asymptotic formula accounts for the r_S^2-versus-φ dependence for $\epsilon\leqslant 0.01$. But the data for $n\leqslant 4$, i.e., for $\epsilon\geqslant 0.05$, are no longer described by the $\sqrt{\sigma}$ law. The range of applicability for the asymptotic description of r_S^2 is remarkably smaller than that for the corresponding description of f_q for intermediate wave numbers [22].

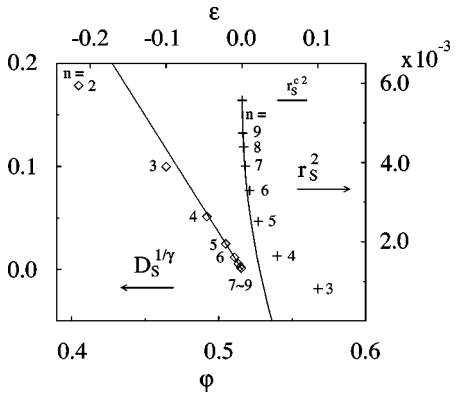

FIG. 3. The diamonds are the values for $D_S^{1/\gamma}$ with the HSS exponent $\gamma=2.46$ for the tagged particle diffusivities D_S determined for the liquid curves in Fig. 2. The straight line is the function $\Gamma(\varphi_c-\varphi)$, $\varphi\leqslant\varphi_c$, with Γ chosen so that the line goes through the data point for $n=9$. The crosses exhibit the square of the localization length, r_S^2, determined for the glass curves in Fig. 2. The full line exhibits the leading asymptotic law $r_S^{c\,2}-h_S\sqrt{\sigma}/\sqrt{1-\lambda}$, Eq. (22).

The glass curve for $\epsilon=0.01$, shown in Fig. 2 with the label $n=6$, exhibits a decay between the end of the transient oscillations and the arrest at r_S^2, which is stretched over a time interval of about two orders of magnitude. A similar two-decade interval is needed for the liquid curve with label $n=6$ to reach the critical value $(r_S^c)^2$. After crossing $(r_S^c)^2$, two further decades of an upward bent $\log_{10}\Delta_S(t)$-versus-$\log_{10}t$ variation are exhibited before the diffusion asymptote is reached. The indicated slow and stretched time variation is referred to as glassy dynamics.

B. The structural-relaxation regime

For times outside the transient regime, say $t\geqslant C^* t_0$, the density correlators can be written in the form $\phi_q(t)=\phi_q^*(t/t_0)$. Here t_0 is the scale introduced in Eq. (16). The functions ϕ_q^* are determined uniquely by the mode-coupling functional $\mathcal{F}_q$, i.e., they are given by the equilibrium structure. This holds for all choices of the regular kernels in Eq. (6), in particular for the two models defined by Eqs. (8a) and (8b) [25,28,30,31]. Corresponding results hold for the density correlators of the tagged atom [30] and of the molecule [25]. The solutions of the specified MCT model for colloids are completely monotone [32]. A function $F(t)$, defined for $t>0$, is called completely monotone if all derivatives exist and

$$(-\partial/\partial t)^n F(t)\geqslant 0,\quad n=0,1,\ldots\ . \tag{23a}$$

According to Bernstein's theorem [33], this property is equivalent to the existence of a distribution $\rho(\gamma)\geqslant 0$ so that

$$F(t)=\int_0^\infty e^{-\gamma t}\,\rho(\gamma)\,d\gamma. \tag{23b}$$

Thus, one can write for $t\geqslant C^* t_0$, $\phi_q(t)=\int_0^\infty e^{-\gamma(t/t_0)}\,\rho_q(\gamma)\,d\gamma$ with $\rho_q(\gamma)\geqslant 0$, i.e., the functions ϕ_q^* deal with relaxation. Corresponding formulas hold for the solute correlators $\phi_q^x(t)$. Representative examples for $\rho_q(\gamma)$ are discussed in Ref. [34].

From Eqs. (5), one gets $C_1(t)=C_1^*(t/t_0)$ for $t\geqslant C^* t_0$, where C_1^* is completely monotone, and also

$$\Delta_x(t)=\Delta_x^*(t/t_0),\quad t\geqslant C^* t_0,\quad x=S,C,A. \tag{24}$$

Here, the functions C_1^* and Δ_x^* are determined by the equilibrium structure. With Eq. (4), one can express the velocity correlator in terms of the structure function $F(\tau)=-\partial_\tau^2\Delta_S^*(\tau)$:

$$K_S(t)=-3\,F(t/t_0)/t_0^2,\quad t\geqslant C^* t_0. \tag{25}$$

It can be shown that the function F is completely monotone. The proof does not provide further insight and is delegated to Appendix A.

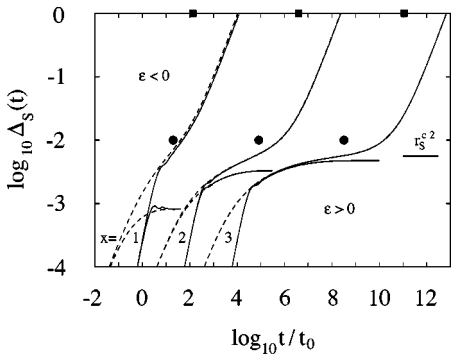

FIG. 4. Double logarithmic presentation of the MSD for a tagged particle of the HSS as a function of the reduced time t/t_0 for distance parameters $\epsilon = \pm 10^{-x}$, $x = 1,2,3$. The full lines reproduce the results from Fig. 2 with labels $n = 3,6,9$ and $t_0 = t_0^H$ from Eq. (21). The dashed lines are the corresponding results for the colloid model specified in the text [23] with $t_0 = t_0^B$ from Eq. (21). The curves for $x = 2$ and 3 are shifted by two and four decades, respectively, to the right to avoid overcrowding. The full dots and squares mark the time scales t_σ and t'_σ, respectively, defined in Eqs. (17c) and (18b).

In Ref. [28], the curves for $\phi_q(t)$ have been compared with the ones for $\phi_q^*(t/t_0)$. The interval for structural relaxation was larger for the colloid model than for the model with the underlying Hamiltonian dynamics. Thus, the structural relaxation interval can be identified as the one where the specified curves for the two models collapse. Figure 4 exhibits such a comparison for the MSD. For $|\epsilon| \leqslant 0.01$, the curves agree within the accuracy of the drawing. This holds, provided $t \geqslant 20t_0$, i.e., $C^* \approx 20$. The result is nearly valid also for distance parameters as large as $|\epsilon| = 0.1$. But there is a small offset between the full and the dashed liquid curves for $x = 1$. This means that there is a smooth drift of t_0 with changes of φ, which is different for the hard-sphere colloid and for the conventional HSS.

In Fig. 5, the rescaled velocity correlator $t_0^2 K_S(t)/3$ for the critical packing fraction is shown as a full line. This diagram is an extension and magnification of the dotted lines from Fig. 1 for $t \geqslant 0.2$. The dashed line is the analogous result $(t_0^B)^2 \partial_t^2 \Delta_S^{\mathrm{col}}(t)$ calculated for the colloid model. The latter function is $(t_0^B D_0^S)^2 F^{\mathrm{col}}(t)$, where the completely monotone function $F^{\mathrm{col}}(t)$ was introduced in Appendix A in connection with Eqs. (A8a) and (A9). According to Eq. (25), the two curves should collapse on the function $F(t/t_0)$. This is the case for $t > 20t_0$ within small error margins. The curves demonstrate stretched relaxation to zero, which cannot be adequately represented on linear scales. It is shown also that oscillatory motion tends to mask glassy relaxation. From now on, the discussion will focus on the structural-relaxation regime $t \geqslant 20t_0$.

C. Scaling-law descriptions

In this section, it shall be examined how well the leading-order asymptotic results from Sec. II C can account quantitatively for the MSD. Let us start with $\Delta_S(t)$ for $\varphi = \varphi_c$. This result for the critical dynamics, i.e., the dotted line in

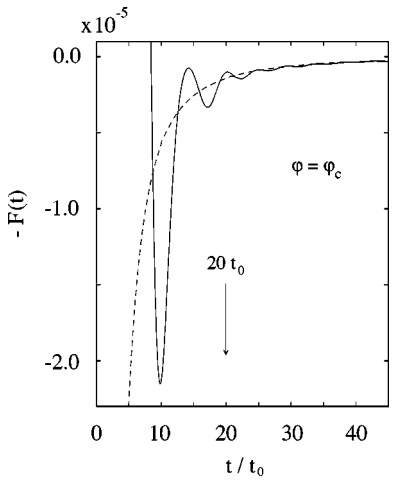

FIG. 5. Rescaled velocity correlators $-F(t) = t_0^2 K_S(t)/3 = t_0^2 \partial_t^2 \Delta_S(t)$ as a function of the rescaled time t/t_0 for a tagged particle of the HSS at the critical packing fraction $\varphi = \varphi_c$. The full line refers to the model for a Hamiltonian dynamics with $t_0 = t_0^H$ from Eq. (21) and the dashed one to the colloid model defined in the text with $t_0 = t_0^B$ from Eq. (21). The full line is a rescaling of the dotted curves in Fig. 1, where values for $t \leqslant 0.2$, i.e., $t/t_0 < 8.5$, are not reproduced.

Fig. 2, is reproduced as a full line in the semilogarithmic presentation in Fig. 6. The transient dynamics for $t \leqslant 20t_0$ accounts for about 45% of the total increase of $\Delta_S(t)$ from zero to the long-time asymptote $r_S^{c\,2}$. The structural relaxation needed to approach $r_S^{c\,2}$ up to 5%, i.e., 50% of the total increase, is stretched over a large interval of about four orders of magnitude time variation. The leading-order formula for the MSD at the transition point is in analogy to Eq. (16),

$$\Delta_S(t) = r_S^{c\,2} - h_S\,(t_0/t)^a, \quad \varphi = \varphi_c, \quad t \gg t_0. \tag{26}$$

The dashed line demonstrates that Eq. (26) describes —

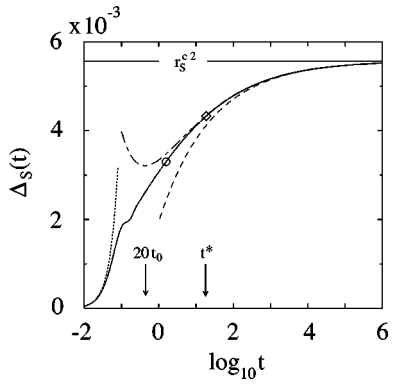

FIG. 6. $\Delta_S(t)$ for a tagged particle of the HSS at the transition point $\varphi = \varphi_c$ (full line), the leading-asymptotic expansion, Eq. (26) (dashed line), and the leading-plus-next-to-leading-asymptotic expansion $\Delta_S(t) = r_S^{c\,2} - h_S(t_0/t)^a + k_S(t_0/t)^{2a}$ (dashed-dotted line). The diamond and circle mark the times $t^* = 18.7 = 792t_0$ and $t^{**} = 1.55 = 65.7t_0$, where the full line differs by 5% from the dashed and dashed-dotted line, respectively. The horizontal line marks the long-time asymptote $r_S^{c\,2}$. The dotted line exhibits the ballistic asymptote $\frac{1}{2}(v_S t)^2$.

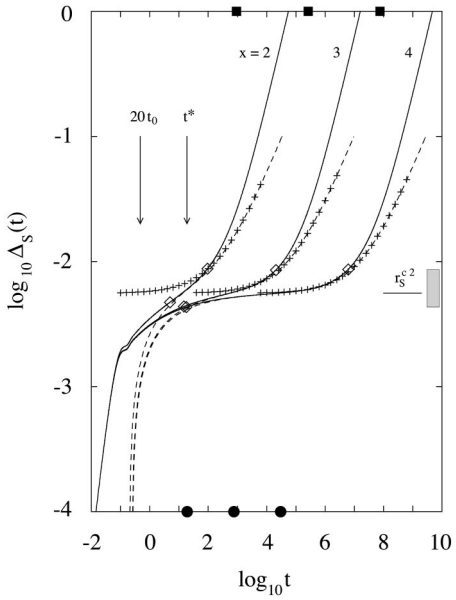

FIG. 7. The full lines show $\Delta_S(t)$ for packing fractions φ given by $\epsilon=(\varphi-\varphi_c)/\varphi_c=-10^{-x}$, $x=2,3,4$. The dashed lines are the first-scaling-law descriptions by Eq. (27). The diamonds mark the points where the dashed lines differ from the full ones by 5%. Within these intervals, $\Delta_S(t)$ varies between about 0.0043 and 0.0086 as is indicated by the shaded bar. The crosses exhibit the von Schweidler law, Eq. (28). The filled circles and squares mark the times t_σ and t'_σ, respectively, defined in Eqs. (17c) and (18b).

within a 5% error margin — about 25% of the total increase of $\Delta_S(t)$. There remains the large part of the structural-relaxation interval between $20t_0$ and $t^*=792t_0$, which is not adequately accounted for. About half of the structural-relaxation increase of $\Delta_S(t)$ is outside the range of applicability of the leading-order asymptotic formula. Extending Eq. (26) by inclusion of the leading correction, one gets a description of the MSD up to errors of order $(t_0/t)^{3a}$: $\Delta_S(t)=(r_S^c)^2-h_S(t_0/t)^a+k_S(t_0/t)^{2a}$. From Ref. [23], one deduces $k_S=0.0143\,d^2$. The dashed-dotted line shows how inclusion of the correction term expands the range of the analytic description.

The first scaling law for the MCT-bifurcation dynamics, Eqs. (17), implies with Eq. (5a),

$$\Delta_S(t)=r_S^{c\,2}-h_S\sqrt{|\sigma|}\,g_\pm(t/t_\sigma),\quad \sigma\gtrless 0,\quad |\sigma|\ll 1,\quad t\gg t_0. \tag{27}$$

For the liquid states with $\sigma<0$, it describes how the $\Delta_S(t)$-versus-t curve crosses the plateau $(r_S^c)^2$. For the glass states with $\sigma>0$, it describes the approach towards the arrest at $r_S^2=\Delta_S(t\to\infty)$. The control-parameter–independent functions $g_\pm(\hat t)$ for the HSS value of λ are discussed in Fig. 10 of Ref. [22]. The dashed lines in Fig. 7 exhibit Eq. (27) for three liquid states. They agree with the MCT solutions within a 5% error margin within the intervals marked by diamonds. Within these intervals, $\Delta_S(t)$ increases from about $0.0043\,d^2$ to about $0.0086\,d^2$. Formulas such as Eqs. (16) and (26) are the basis for the derivation of the MCT-scaling laws. Therefore, it follows from Fig. 6 that the part of the structural relaxation regime between $20t_0$ and t^* remains outside the range of validity of Eq. (27).

For small rescaled times $\hat t=t/t_\sigma$, Eq. (27) reproduces Eq. (26) for $\sigma\to 0$. The right-hand side of Eq. (27) becomes independent of σ and agrees with Eq. (26). This explains why the dashed lines in Fig. 7 for $x=3$ and 4 collapse for $t\leqslant 10$ and why the corresponding diamonds are located near t^*. For $x=2$, the separation parameter σ is already so large that $g_\pm(t^*/t_\sigma)$ differs remarkably from $(t_\sigma/t^*)^a$. Therefore, $\Delta_S(t)$ does not reach the t^{-a} asymptote for $t\approx t^*$, and the corresponding diamond shifts away from t^*. The $x=3$ curve follows the critical asymptote from Eq. (26) for a time interval of less than two decades. Such an interval would not be large enough for a compelling experimental confirmation of the t^{-a} law. To identify the t^{-a} law in its pure form for the model under study, $|\epsilon|$ must not exceed 10^{-4}.

For large rescaled times $\hat t$, the master function for the glass approaches $g_+(\hat t\to\infty)=1/\sqrt{1-\lambda}$, and Eq. (27) reproduces Eq. (22). According to the preceding paragraphs, this explains the solutions for the glass provided the long-time limit r_S^2 is located in the shaded interval of Fig. 7, and this is demonstrated in Fig. 3.

Function $g_-(\hat t)$ for the liquid is zero for $\hat t_-=0.704$. Thus, $\Delta_S(\hat t_- t_\sigma)=(r_S^c)^2$ and the interval for the increase of $\Delta_S(t)$ to the plateau value $(r_S^c)^2$ expands proportional to t_σ if φ increases towards φ_c. For large $\hat t$, one gets von Schweidler's law,

$$\Delta_S(t)=(r_S^c)^2+h_S\,(t/t'_\sigma)^b,\quad \sigma\to -0,\quad t_\sigma\ll t\ll t'_\sigma. \tag{28}$$

Therefore, the long-time end of the range of applicability of Eq. (27) expands proportional to t'_σ, as is indicated by the filled squares in Fig. 7. Formula (28) is exhibited by the crosses. These approach the plateau $r_S^{c\,2}$ for $t\ll t_\sigma$ and the dashed scaling-law lines for $t\gg t_\sigma$. Since $t'_\sigma/t_\sigma\to\infty$ for $|\epsilon|\to 0$, the time interval for the von Schweidler–law description expands with decreasing $|\epsilon|$.

Equation (17a) formulates the factorization theorem for $\delta\phi_A(t)=\phi_A(t)-f_A^c$: in a leading-order expansion for small $\delta\phi_A$, the deviation $\delta\phi_A(t)$ of the correlator from the plateau value f_A^c factorizes in a control-parameter–independent amplitude h_A and a function $G(t)$. The function $G(t)$ is the same for all variables A and describes the time-and-control-parameter dependence of $\phi_A(t)$ by a scaling law, Eq. (17b). This theorem can be tested by identifying the time interval and the range of distance parameters ϵ for which the diagrams for $\hat\phi_A(t)=\delta\phi_A(t)/h_A$ collapse with $G(t)$. Figure 8 demonstrates such a test for the dipole correlators $C_1(t)$ for three values of the elongation parameter ζ. The markers for $20t_0$, t^*, t_σ, and t'_σ have been added to facilitate a comparison with Fig. 7. Obviously, the scenario for the plateau crossing is the same for $C_1(t)$ as discussed above for $\Delta_S(t)$. To corroborate this conclusion, the rescaled result for the MSD, $\hat\Delta_S(t)=[r_S^{c\,2}-\Delta_S(t)]/h_S$ for $\epsilon=-0.001$, has been added to the figure. The $x=2$ results show that for negative $\hat C_1(t)$, the full lines follow the sequence $\zeta=$ 0.6, 0.8, and 1.0

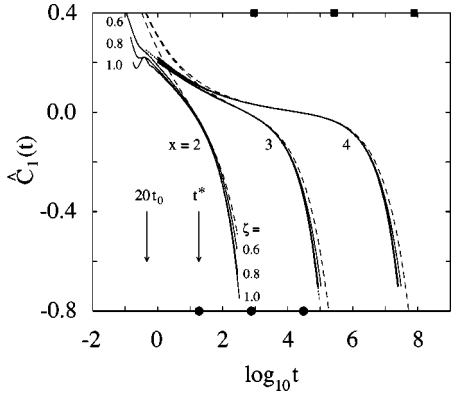

FIG. 8. The full lines are dipole correlators $C_1(t)$ rescaled to $\hat{C}_1(t)=[C_1(t)-f_1^c]/h_1$ for the elongation parameters $\zeta=0.6$, 0.8, and 1.0 (from top to bottom), where $f_1^c=0.769,0.905,0.955$ and $h_1=0.46,0.19,0.09$, respectively. The distance parameters are $\epsilon=-10^{-x}$, $x=2,3,4$ (compare text). The filled circles and squares mark the times t_σ and t'_σ, respectively, for the three packing fractions. The dashed lines exhibit the first-scaling-law asymptotes $\sqrt{|\sigma|}g_-(t/t_\sigma)$. The dotted line is the MSD for a tagged particle for $x=3$ rescaled to $\hat{\Delta}_S(t)=[r_S^{c\,2}-\Delta_S(t)]/h_S$.

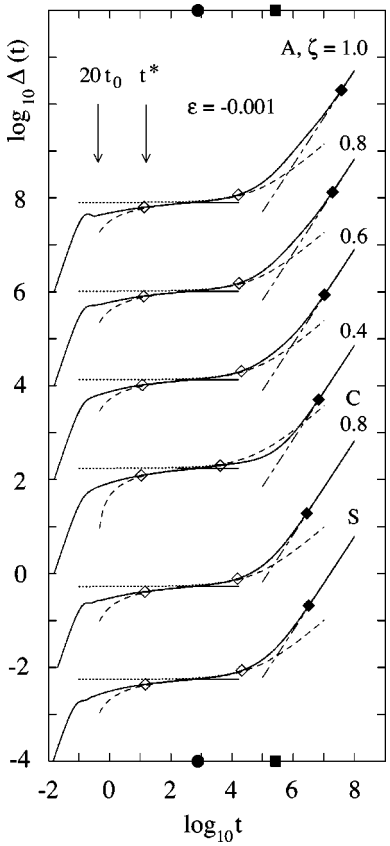

FIG. 9. $\Delta_S(t)$ and $\Delta_C(t)$ for $\zeta=0.8$, and $\Delta_A(t)$ for $\zeta=0.4$, 0.6, 0.8, 1.0 (full lines, from bottom to top). Successive curves are shifted upwards by two decades to avoid overcrowding. The distance parameter is $\epsilon=-10^{-3}$ and the corresponding times t_σ and t'_σ are marked by filled circles and squares, respectively. The dashed lines are the first-scaling-law asymptotes, Eq. (27). The open diamonds mark the points where the dashed lines differ from the full ones by 5%. The straight dashed-dotted lines exhibit the diffusion asymptotes D_St, D_Ct, and D_At, and the filled diamonds mark the position where these differ from the full lines by 5%. The dotted lines, which coincide with the full ones for $t\geqslant 10^4$, exhibit the second-scaling-law asymptotes, Eq. (29).

from top to bottom, where the latter two curves are very close to each other. The same behavior is observed for positive $\hat{C}_1(t)$. This observation exemplifies a general implication of the leading corrections to the factorization theorem [22].

A possibility for the definition of a characteristic time scale τ_A for the α process of variable A is given by the time needed to complete 95% of the total decay from the plateau f_A^c to the equilibrium value zero, i.e., $\phi_A(\tau_A)=f_A^c/20$. Within the range of validity of the second scaling law, Eq. (19), the A-dependent scales are coupled in the sense that $\tau_A=\tilde{\tau}_A\,t'_\sigma$. Here $\tilde{\tau}_A$ is an A-specific control-parameter–independent factor determined by $\tilde{\phi}_A(\tilde{\tau}_A)=f_A^c/20$. Applying these results to the dipole correlator, one gets $C_1(t)=\tilde{C}_1(\tilde{t})$ for $|\sigma|\ll 1$ and $t_\sigma\ll t$, where $\tilde{t}=t/t'_\sigma$. For the α-scale factors, one finds $\tilde{\tau}_1=18.8$ (8.73,2.66) for $\zeta=1.0$ (0.8,0.6). The description of the α process for elongation parameter $\zeta=0.8$ is demonstrated in Fig. 8 of Ref. [35].

Using the second scaling law for the tagged-particle-density correlator, one gets from Eq. (5a) the second scaling law for the α process of the MSD,

$$\Delta_S(t)=\tilde{\Delta}_S(\tilde{t}),\quad \tilde{t}=t/t'_\sigma,\quad |\sigma|\ll 1,\quad t_\sigma\ll t. \tag{29}$$

An α-relaxation time τ_S shall be defined by that time, where the diffusion asymptote $D_S\,t$ is reached within 5%, i.e., $\Delta_S(\tau_S)=1.05\,D_S\,\tau_S$. One gets $D_S=\tilde{D}_S/t'_\sigma$ and $\tau_S=\tilde{\tau}_S\,t'_\sigma$, where $\tilde{D}_S$ and $\tilde{\tau}_S$ are to be determined from $\lim_{\tilde{t}\to\infty}\tilde{\Delta}_S(\tilde{t})/\tilde{t}=\tilde{D}_S$ and $\tilde{\Delta}_S(\tilde{\tau}_S)/\tilde{\tau}_S=1.05\tilde{D}_S$. One finds $\tilde{D}_S=0.0171$ and $\tilde{\tau}_S=11.6$. One gets in particular $D_S\propto 1/t'_\sigma\propto(\varphi_c-\varphi)^\gamma$, and Fig. 3 demonstrates how the diffusivity approaches this power-law asymptote for φ increasing to φ_c. The asymptotic description of $\Delta_S(t)$ by Eq. (29) is demonstrated in Fig. 9 of Ref. [23].

For times of order t_σ, the relative corrections to the first scaling law are of order $\sqrt{|\sigma|}$. For times of order t'_σ, the corrections to the second scaling law are of order $|\sigma|$. Therefore, the second scaling law holds for larger separations $|\sigma|$ than the first one [22]. For example, even for the large value $\epsilon=-0.1$, $D_S^{1/\gamma}$ differs from the linear asymptote by only 15%, as is demonstrated by the $n=3$ result in Fig. 3. The corrections to Eq. (29) increase if t decreases towards t_σ. But for $t\approx t_\sigma$, the description in terms of the first scaling law becomes valid, which provides the leading corrections to Eq. (29). The descriptions in terms of the two scaling laws overlap. Together, they provide a complete description of the dynamics for $t\geqslant t^*$. This holds provided $|\epsilon|$ is small enough, as is demonstrated in Fig. 9 for $\epsilon=-10^{-3}$ for $\Delta_S(t)$ and $\Delta_C(t)$ for $\zeta=0.8$, and for $\Delta_A(t)$ for four values of ζ. From

the analogous figure constructed for $\epsilon=-10^{-2}$, one concludes that the scaling-law description accounts for the MSD quantitatively for $t\geqslant t^*$ and $|\epsilon|\leqslant 0.01$. For larger distance parameters, corrections to scaling become visible.

D. Rotation-translation-coupling effects

It might be adequate to start the discussion of rotation-translation-coupling effects with two side remarks. First, it was shown that the correlators for the dipole and the quadrupole dynamics for $\zeta=0.8$ are in semiquantitative agreement with the experimental data for propylene carbonate [35]. Thus, the results to be discussed for $\zeta\geqslant 0.6$ can be considered relevant for the interpretation of glass-forming van-der-Waals liquids. Second, the system under study exhibits two glass phases for $\varphi\geqslant\varphi_c$. There is a critical elongation ζ_c so that for $\zeta>\zeta_c$, correlations of the molecule's axis arrest for long times as do all other correlations of variables characterizing the structure. In particular, $C_1(t\to\infty)=f_1>0$. But for $\zeta\leqslant\zeta_c$, dipole correlations exhibit ergodic behavior, i.e., $C_1(t\to\infty)=0$. Precursor effects of this glass-glass transition at ζ_c disturb the standard transition scenario [25,35]. This is the reason why $\Delta_A(t)$ for $\zeta=0.4$ is remarkably different from $\Delta_A(t)$ for the other ζ shown in Fig. 9; for $\zeta=0.4$, the elongation is too close to $\zeta_c=0.380$. For example, for $\zeta=0.4$, the corrections to von Schweidler's law, which shift the dashed lines onto the full ones for $t_\sigma<t<t'_\sigma$, are negative, while they are positive for the other cases.

The glass transition of the HSS is driven by density fluctuations with wave numbers near the first-peak position of the structure factor S_q close to $q=7.0/d$. For the scale factor for the α process of these fluctuations, defined by $\tilde{\phi}_q(\tilde{\tau}_q)=f_q^c/20$, one gets $\tilde{\tau}_{7.0}=6.0$. For the α relaxation of the tagged-particle-density correlations for the same wave vector, one gets a similar number $\tilde{\tau}^S_{7.0}=5.0$. One concludes that the α-scale factor $\tilde{\tau}_S=\tau_S/t'_\sigma=11.6$ for the approach of $\Delta_S(t)$ to the diffusion limit is in the range within which relevant density fluctuations decay to zero. The corresponding interval for the crossover from the end of the von Schweidler decay to the beginning of diffusion is 2.2 decades. This is shown by the lowest curve in Fig. 9 and should be considered as the normal behavior for the density-fluctuation dynamics in simple systems. The MSD for the molecule's center behaves quite similarly; $\Delta_C(t)$ for $\zeta=0.8$ is nearly indistinguishable from $\Delta_S(t)$. However, Fig. 9 demonstrates also that $\Delta_A(t)$ behaves differently. For $\zeta=1.0$ (0.8,0.6), the above-specified crossover intervals are 3.3 (3.1,2.8) decades wide. This means that the crossover intervals of $\Delta_A(t)$ are larger than those of $\Delta_S(t)$ or $\Delta_C(t)$ by factors of about 13 (7,4), and so are the α scales τ_A compared to τ_S or τ_C. The reason is the reorientational contribution to the MSD of the constituent atom, i.e., the second term on the right-hand side of Eq. (2). There are two effects. First, for $t/t'_\sigma\gg\tilde{\tau}_1$, the dipole correlations are decayed to zero, i.e., the molecule's axis is distributed on the unit sphere with a constant probability density. Therefore, there is the positive offset $X=(\zeta d)^2/12$ between the two functions referring to the atom and the center. $\Delta_A(t)-\Delta_C(t)=X$ for $\tilde{t}=t/t'_\sigma\geqslant\tilde{\tau}_1$ as is demonstrated in the linear representation of the α-process master functions in Fig. 10. The slow decay of the relative offset X/D_Ct explains that the ratio $\tilde{\tau}_A/\tilde{\tau}_C$ is larger than unity, increasing in conjunction with ζ. Second, steric hindrance for reorientations increases with ζ. For $\zeta>0.8$, the α scale $\tilde{\tau}_1$ for dipole relaxations becomes comparable to or larger than $\tilde{\tau}_C$. Therefore, there appears an interval $1<t/t'_\sigma<\tilde{\tau}_1$, after the end of the von Schweidler–law regime and before the beginning of the diffusion regime, where the $\Delta_A(t)$-versus-t diagram, in contrast to the $\Delta_C(t)$-versus-t one, exhibits a curvature. This is shown for $\zeta=0.8$ and 1.0 in Fig. 10.

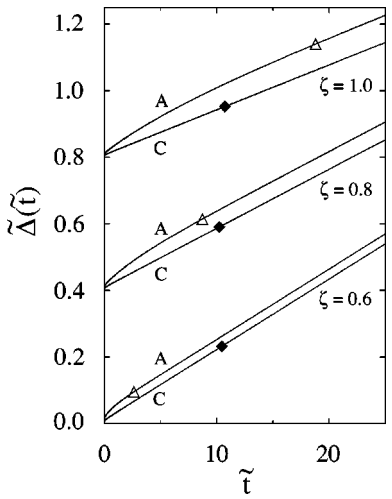

FIG. 10. α-relaxation master functions $\tilde{\Delta}$ as a function of the rescaled time $\tilde{t}=t/t'_\sigma$ for $\zeta=1.0$, 0.8, and 0.6 (from top to bottom). The curves for $\zeta=0.8$ (1.0) are shifted upward by 0.4 (0.8) in order to avoid overcrowding. Curves with labels C and A refer to the MSD for the molecule's center and for the constituent atom, respectively. The filled diamonds mark the time $\tilde{\tau}_C$, where the diffusion asymptote is reached within 5%: $\tilde{\Delta}_C(\tilde{\tau}_C)=1.05\tilde{D}_C\tilde{\tau}_C$. The corresponding time $\tilde{\tau}_A$ for the constituent atom for $\zeta=1.0(0.8,0.6)$ is $\tilde{\tau}_A=140(72,39)$. The triangles mark the time $\tilde{\tau}_1$, where the dipole correlator has completed 95% of its α decay: $\tilde{C}_1(\tilde{\tau}_1)/f_1=0.05$.

If a hard sphere gets expanded to a dumbbell with a small elongation, the molecule's center gets restricted more tightly in its cage. Therefore, provided ζ is small, the localization length r_C^c is smaller than r_S^c and it decreases with increasing ζ. For $\zeta\approx 1.0$, the localization of one constituent atom of the molecule restricts the motion of its partner. Therefore, r_C^c is smaller than r_S^c also for large elongations. Counterintuitively, the theory does not lead to a monotonic interpolation between the specified limits. The $r_C^{c\,2}$-versus-ζ diagram in Fig. 11 exhibits an oscillation and r_C^c exceeds r_S^c by about 10% for ζ near 0.6.

For $\zeta\leqslant\zeta_c$, one gets $C_1(t\to\infty)=0$. If one neglects the variation of the $r_C^{c\,2}$-versus-ζ curve, Eq. (2) leads to $r_A^{c\,2}=r_S^{c\,2}+(\zeta d)^2/12$. The dotted line in Fig. 11 shows that this formula explains the increase of r_A^c for ζ increasing up to ζ_c. For ζ increasing above ζ_c, the decrease of $1-f_1$ and of r_C^c explains the decrease of r_A^c.

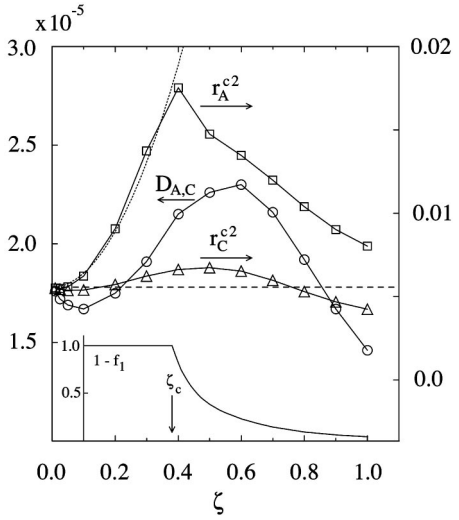

FIG. 11. Squares and triangles are the localization lengths squared at the transition point $\varphi=\varphi_c$ as a function of the molecule's elongation ζ for the constituent atom ($r_A^{c\,2}$) and the center ($r_C^{c\,2}$), respectively. The circles are the diffusivity $D_A=D_C$ of the molecule calculated for $\epsilon=-0.01$. The lines connecting the symbols are guides to the eye. The horizontal dashed line is a common one indicating both the values of the square of the localization length $r_S^{c\,2}$ (on the right scale) and of the diffusivity D_S (on the left scale) for a tagged particle of the HSS. The dotted line is the function $r_S^{c\,2}+(\zeta d)^2/12$ discussed in the text. The inset exhibits $1-f_1$ as a function of ζ, where $f_1=C_1(t\to\infty)$ is the long-time limit of the dipole correlator $C_1(t)$. The arrow indicates the critical elongation $\zeta_c=0.380$ for a glass-glass transition.

It seems plausible that the number of paths for the molecule through the system's configuration space decreases with increasing elongation. Therefore, one might expect that the diffusivity $D_A=D_C$ is smaller than D_S and decreases with increasing ζ. Figure 11 confirms this expectation for small and for large elongations. But, strangely, the calculated diffusivity is not a monotone function of ζ, and for $\zeta\approx 0.6$, D_C exceeds D_S by about 30%.

IV. CONCLUSIONS

MCT predicts that the long-time parts of the density-correlation functions $\phi_q(t)$ of the solvent and $\phi_q^x(t)$ of the solute deal with relaxation in the sense that they are superpositions of Debye-relaxation processes $\exp[-\gamma(t/t_0)]$. They deal with structural dynamics in the sense that the weight functions $\rho_q(\gamma)$ and $\rho_q^x(\gamma)$ for these superpositions are uniquely determined by the equilibrium structure. The corresponding dynamics is therefore referred to as structural relaxation. Within the structural-relaxation regime, the subtleties of the normal-liquid dynamics merely enter via the value for an overall time scale t_0, which is defined with the aid of the critical decay law, Eq. (16). The structural-relaxation interval was estimated for the hard-sphere system (HSS) under study as $t>20t_0$ (Sec. III B, Fig. 4). The specified properties of the MCT dynamics are asymptotic ones, valid for large times near the transition point. The estimation of the range of validity depends on the accuracy level required and also on the particular function under discussion Differentiation with respect to time, as is considered in Eq. (4) for the velocity correlator $K_S(t)$, enhances oscillation features, i.e., deviations from relaxation behavior. Figure 5 demonstrates indeed that one would estimate the structural relaxation interval for $K_S(t)$ as $t>40t_0$, i.e., somewhat more restrictive than for the MSD.

For a normal liquid, the velocity correlator is positive for short times. It is also positive for times exceeding a crossover time t_h, where it exhibits a hydrodynamic long-time tail proportional to $t^{-3/2}$ [1]. But, upon approaching the glass-transition point, the regime for hydrodynamics shrinks to lower frequencies. Therefore, the time t_h diverges if the packing fraction φ approaches the critical value φ_c. The cage effect causes $K_S(t)$ to be negative for $t>20t_0$. Even more, the correlation of the particle velocity at time t with a value opposite that of its initial value, say $\Psi(t)=\langle\vec{v}_S(t)\cdot[-\vec{v}_S(t=0)]\rangle$, is proportional to a completely monotone function $F(t/t_0)$, Eq. (25). The function Ψ represents a relaxation process in the sense of Eq. (23b), where the weight function $\rho(\gamma)$ is given by the structural function. These results for the velocity correlator for $t>20t_0$ express concisely the essence of glassy dynamics, namely the relaxation caused by the cage effect and determined by the Boltzmann factors for the equilibrium structure.

The MSD increases with time according to the characteristic two-step pattern of the MCT-transition scenario. There is a stretched approach towards a plateau value $r_S^{c\,2}$ followed by arrest at the square of the localization length $r_S^2<r_S^{c\,2}$ within the glass or by the stretched start of the α process within the liquid, Fig. 2. The sensitive density dependence of the MSD near the plateau is described by the universal formulas for the first scaling law, as is demonstrated in Fig. 7. The same holds for the dipole correlator $C_1(t)$. This is shown in Fig. 8 by scaling $C_1(t)$ for three values of the molecule's elongation on the same functions $\sqrt{|\sigma|}\,g_-(t/t_\sigma)$. However, there is a large time interval at the beginning of the structural-relaxation regime, $20t_0<t<t^*\approx 800t_0$, where the universal leading-order-asymptotic formulas do not describe the MSD, as is shown in Figs. 6 and 7. The theory predicts similar results for all systems with a structure similar to that of the HSS, i.e., for all van-der-Waals liquids. Obviously, it would be worthwhile to test by experiment or molecular-dynamics simulation whether the specified prediction is correct, and in particular whether MCT can reproduce properly the structural relaxation of the MSD outside the scaling-law regime.

The beginning of the α process of the MSD, i.e., the increase of $\Delta_x(t)$ above the plateau $r_x^{c\,2}$, is described by von Schweidler's law, Eq. (28). It is exhibited in Fig. 9 for $t>t_\sigma$ by the dashed lines. The α process terminates in the diffusion law for long times, exhibited in Fig. 9 by the straight dashed-dotted lines. The α process follows well the second scaling law, Eq. (29), which is presented by the dotted lines. The crossover interval from the end of the von Schweidler–law description (indicated by the open diamonds) to the beginning of the diffusion process (indicated by the filled diamonds) for the MSD of an atom is about two

decades wide, as shown by the lowest curve in Fig. 9. The same is true for the MSD of the molecule's center. But the crossover interval for the MSD of the constituent atom of the molecule is much larger due to the rotation-translation coupling. The expansion is more than an order of magnitude for $\zeta=1.0$. It would be valuable for an assessment of the MCT for molecular systems if this prediction could be tested by molecular-dynamics simulation.

Bennemann *et al.* [36] have determined by molecular-dynamics simulation the MSD for the monomer and for the center of a polymer for a model of a glassy polymer melt. They identified for their data the α process in the sense of MCT and interpreted it consistently with the universal asymptotic formulas. They observed the expansion of the crossover interval for the monomer MSD relative to that for the center, similar to what is shown in Fig. 9 for $\zeta=1.0$, and they attribute this expansion to the glassy dynamics of the Rouse modes. These modes for the polymer's internal degrees of freedom are thus identified as part of the α process [36]. Figures 9 and 10 corroborate their conclusions, albeit for the simplest polymer model only, namely a rigid hard-sphere dimer.

Let us consider a one-dimensional model, where two hard spheres are restricted to move in a finite interval. One calculates easily the localization length r_S of one of the spheres, assuming the other sphere moves freely between the wall and its partner. Similarly, one can calculate the localization length r_C of the center of a dumbbell built by the two spheres. One finds $r_C>r_S$, i.e., the freely moving partner provides a stronger hindrance for the motion in the cage than the bonded one. Possibly, the result $r_C^c>r_S^c$ shown in Fig. 11 for $\zeta\simeq0.6$ is the analog of this phenomenon for one-dimensional localization. To corroborate this reasoning, Fig. 12 exhibits as full lines the isotropic part $g_0^S(r)$ of the solute-solvent pair distribution function and the corresponding structure factor $S_0^S(q)$ for $\varphi=\varphi_c$ for a dumbbell with $\zeta=0.6$ [29]. The dashed lines exhibit the results for a sphere with diameter $d_{\rm eff}=1.215\,d$ chosen such that its volume agrees with that of the dumbbell. The well-known excluded-volume effects for this effective spherical solute are larger than those for the tagged particle of the HSS. In particular, the structure factor peak is higher. Therefore, the localization length $r_{\rm eff}^c=0.0588\,d$ for the effective spherical solute is much shorter than the localization length $r_S^c=0.0746\,d$ for the tagged particle of the HSS. The ratio $r_{\rm eff}^c/r_S^c$ decreases with increasing ζ. The pair distribution function of the effective sphere agrees reasonably well with $g_0^S(r)$ for the dumbbell for $r>1.5\,d$. Therefore, the two structure factors are close to each other on the wings of the $S_0^S(q)$ peaks and also for small q. However, packing cannot be done as efficiently around the dumbbell as around a sphere of the same volume. Therefore, the pair distribution function for the latter is much bigger for r near $d_{\rm eff}$ than $g_0^S(r)$ for the dumbbell. This depletion effect leads to a reduction of $|S_0^S(q)|$ at the peak position and also for larger wave numbers. Hence, the depletion reduces the magnitude of the mode-coupling coefficients. As a result, the localization length $r_0^c=0.0863\,d$, calculated by using MCT equations for a simple system with only the isotropic part of the dumbbell structure factor, is not only larger than $r_{\rm eff}^c$, but it is even larger than r_S^c. The estimated r_0^c is rather close to the true localization length $r_C^c=0.0808\,d$ for the dumbbell's center. Only if ζ becomes even larger do mode couplings to the nonisotropic parts of the density fluctuations take over and compensate for the depletion effects. This leads to the decrease of r_C^c with increasing ζ for $\zeta>0.6$, as shown in Fig. 11.

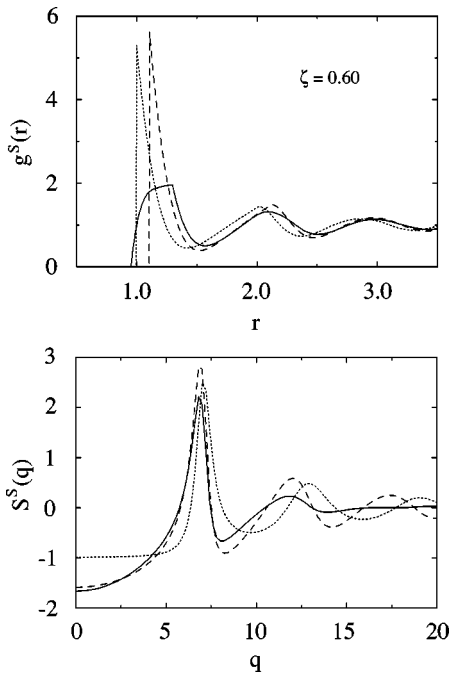

FIG. 12. Pair distribution $g^S(r)$ as a function of the distance r between solvent particles and the center of the solute (upper panel) and the corresponding solute-solvent structure factor $S^S(q)$ (lower panel) calculated within the Percus-Yevick theory for the critical packing fraction $\varphi_c=0.516$. The dotted lines refer to a tagged sphere of the same diameter, $d_S=d$, as the one of the solvent particles. The dashed lines refer to a spherical solute of diameter $d_{\rm eff}=1.215\,d$ (see the text). The full lines exhibit the isotropic part of the distribution $g_0^S(r)$ and the structure factor $S_0^S(q)$ for a dumbbell consisting of two fused hard spheres of diameter d with the elongation $\zeta=0.6$ [29].

The above-discussed depletion effect means that the dumbbell is surrounded by a liquid of lower averaged density than specified by the packing fraction. Hence, the dumbbell moves in a complex, which effectively has a larger distance from the glass-transition point than is specified by $(\varphi_c-\varphi)/\varphi_c$. Such a lubrication phenomenon for the dumbbell in the complex might explain the increase of the diffusivity exhibited in Fig. 11 for $\zeta\sim0.6$. Diffusion in a dense liquid is a collective phenomenon. A particle can move over a distance comparable to its diameter only if one of its neighbors moves. This neighbor can move only if its neighbor moves, and so on. On the average, a flow pattern will be built similar to the motion of a sphere in an incompressible ideal liquid. It was one of the original motivations for the formulation of the MCT equation of motion to treat approximately the indicated backflow phenomenon. Molecular-dynamics simulation has

shown that a typical event underlying the mentioned averaged backflow pattern might consist of quasi-one-dimensional motions of clusters of particles [37]. It seems possible that the bonding of two atoms to a molecule stabilizes the cluster, provided the elongation ζd is smaller than the diameter of the ring formed by the moving cluster. If this were the case, the diffusivity for the molecule should be larger than that for a tagged atom. Hence, it is not obvious that the nonmonotone variation of the diffusivity with changes of ζ, which is shown in Fig. 11, is a mere artifact of the approximations underlying the presented theory.

ACKNOWLEDGMENTS

We thank M. Fuchs, W. Kob, M. Sperl, W. van Megen, and Th. Voigtmann for helpful and stimulating discussions. S.-H.C. acknowledges financial support from the Japan Society for the Promotion of Science. This work was supported by Verbundprojekt BMBF 03-G05TUM.

APPENDIX: MODE-COUPLING-THEORY MODELS FOR COLLOIDS

In this appendix, it will be shown how the MCT formulas for simple systems can be specialized to models for the dynamics of colloids. Within this frame, a representation of the velocity correlator in terms of a completely monotone function $F^{\mathrm{col}}(t)$ will be derived. To begin, let us remember the definition of Laplace transforms of functions of time, say $F(t)$, to functions of the complex frequency s: $F(s) = \int_0^\infty dt \exp(-st) F(t)$. Applying this transformation to $\phi_q(t)$, $M_q^{\mathrm{reg}}(t)$, and $m_q(t)$, one can rewrite Eq. (6) together with the initial conditions $\phi_q(t=0)=1$ and $\partial_t \phi_q(t=0)=0$ as a double fraction for $\phi_q(s)$:

$$\phi_q(s) = 1 / \{ s + \Omega_q^2 / [s + M_q^{\mathrm{reg}}(s) + \Omega_q^2 m_q(s)] \}. \quad \text{(A1)}$$

The analogous result can be obtained for the tagged-particle correlator,

$$\phi_q^S(s) = 1 / \{ s + (q v_S)^2 / [s + M_q^{S,\mathrm{reg}}(s) + (q v_S)^2 m_q^S(s)] \}. \quad \text{(A2)}$$

Equation (4) can be rewritten as a relation between the Laplace transforms $\Delta_S(s)$ and $K_S(s)$ of $\Delta_S(t)$ and $K_S(t)$, respectively:

$$K_S(s) = 3 s^2 \Delta_S(s). \quad \text{(A3)}$$

The small-q expansion of Eq. (A2) leads to

$$K_S(s) = 3 v_S^2 / [s + M_0^{S,\mathrm{reg}}(s) + v_S^2 m_S(s)]. \quad \text{(A4)}$$

Here $M_0^{S,\mathrm{reg}}(s) = \lim_{q\to 0} M_q^{S,\mathrm{reg}}(s)$, and $m_S(s) = \lim_{q\to 0} q^2 m_q^S(s)$ is the transform of $m_S(t)$ from Eq. (14a) [12].

In a colloid, there is a contribution to the fluctuating force due to the interaction of the particles with the suspending liquid. This leads to contributions to the rates $M_q^{\mathrm{reg}}(s)$ and $M_q^{S,\mathrm{reg}}(s)$, which are large compared to the scale for the frequency s one wants to consider. Therefore, it is the conventional first approximation step of a theory for colloid dynamics to coarse-grain correlation functions on time scales of the order of $1/M_q^{\mathrm{reg}}(s)$ and $1/M_q^{S,\mathrm{reg}}(s)$. For the correlators considered here, this means that $s + M_q^{\mathrm{reg}}(s)$ in Eq. (A1), $s + M_q^{S,\mathrm{reg}}(s)$ in Eq. (A2), and $s + M_0^{S,\mathrm{reg}}(s)$ in Eq. (A4) are replaced by $\nu_q = M_q^{\mathrm{reg}}(s=0)$, $\nu_q^S = M_q^{S,\mathrm{reg}}(s=0)$, and $\nu_0^S = M_0^{S,\mathrm{reg}}(s=0) = \lim_{q\to 0} \nu_q^S$, respectively. Let us indicate the various functions, obtained by this specialization of MCT, by superscripts ''col.'' The equations of motion, obtained by the backtransformation of the so-modified Eqs. (A1) and (A2), are [22,23]

$$\tau_q \partial_t \phi_q^{\mathrm{col}}(t) + \phi_q^{\mathrm{col}}(t) + \int_0^t dt' \, m_q^{\mathrm{col}}(t-t') \, \partial_{t'} \phi_q^{\mathrm{col}}(t') = 0, \quad \text{(A5)}$$

$$\tau_q^S \partial_t \phi_q^{S,\mathrm{col}}(t) + \phi_q^{S,\mathrm{col}}(t) + \int_0^t dt' \, m_q^{S,\mathrm{col}}(t-t') \, \partial_{t'} \phi_q^{S,\mathrm{col}}(t') = 0. \quad \text{(A6)}$$

Here $\tau_q = \nu_q / \Omega_q^2$ and $\tau_q^S = \nu_q^S / (q v_S)^2$ are times characterizing conventional colloid dynamics. The interaction potentials between the particles, which cause the cage effect, are not altered by the introduction of the solvent. Therefore, the expressions for the mode-coupling contributions to the kernels, Eqs. (7) and (9), keep their functional form,

$$m_q^{\mathrm{col}}(t) = \mathcal{F}_q[\phi_k^{\mathrm{col}}(t)], \quad m_q^{S,\mathrm{col}}(t) = \mathcal{F}_q^S[\phi_k^{S,\mathrm{col}}(t), \phi_p^{\mathrm{col}}(t)]. \quad \text{(A7)}$$

Equations (A5)–(A7), together with the initial conditions $\phi_q^{\mathrm{col}}(t=0)=1$ and $\phi_q^{S,\mathrm{col}}(t=0)=1$, define a unique solution with all the general properties of correlation functions [32]. Since the coarse graining has altered the $s\to\infty$ asymptote of the correlator transforms relative to that exhibited by Eqs. (A1) and (A2), the short-time behavior is altered, namely $\phi_q^{\mathrm{col}}(t\to 0) = 1 - |t|/\tau_q + \cdots$, $\phi_q^{S,\mathrm{col}}(t\to 0) = 1 - |t|/\tau_q^S + \cdots$. Since s was dropped in the denominator of Eq. (A4), the velocity-correlator Laplace transform for the colloid dynamics does not tend to zero for large s; rather $K_S^{\mathrm{col}}(s\to\infty) = 3 D_0^S$, with the abbreviation $D_0^S = v_S^2 / \nu_0^S$. This suggests rewriting the coarse-grained velocity correlator as

$$K_S^{\mathrm{col}}(s)/3 = D_0^S - D_0^{S\,2} F^{\mathrm{col}}(s), \quad \text{(A8a)}$$

$$F^{\mathrm{col}}(s) = m_S^{\mathrm{col}}(s) / [1 + D_0^S m_S^{\mathrm{col}}(s)], \quad \text{(A8b)}$$

$$m_S^{\mathrm{col}}(t) = \mathcal{F}^S[\phi_k^{S,\mathrm{col}}(t), \phi_p^{\mathrm{col}}(t)]. \quad \text{(A8c)}$$

The solutions of Eqs. (A5)–(A7) are completely monotone [32]. Kernel $m_S^{\mathrm{col}}(t)$ is a combination with positive coefficients of products of completely monotone functions because of Eqs. (A8c) and (14), and therefore it is completely monotone as well [33]. Because of Bernstein's theorem, one can write $m_S^{\mathrm{col}}(s) = \int_0^\infty [s+\gamma]^{-1} \rho(\gamma) d\gamma$ with a non-negative distribution $\rho(\gamma)$. Therefore, the following four properties hold [33] for $m_S^{\mathrm{col}}(s)$: (i) it is holomorphic for all complex s, except for negative real numbers; (ii) $m_S^{\mathrm{col}}(s)^* = m_S^{\mathrm{col}}(s^*)$;

(iii) $m_S^{\rm col}(s)\to 0$ for $\mathrm{Re}\, s\to\infty$; and (iv) $\mathrm{Im}\, m_S^{\rm col}(s)<0$ for $\mathrm{Im}\, s>0$. One concludes furthermore that $1+D_0^S m_S^{\rm col}(s)\neq 0$ for all s except, possibly, negative real values. From Eq. (A8b) one concludes that also $F^{\rm col}(s)$ exhibits the properties (i)–(iv). Hence, $F^{\rm col}(s)$ is the Laplace transform of a completely monotone function $F^{\rm col}(t)$ (Ref. [33], Chap. 5, theorem 2.6). The backtransformation of Eq. (A8a) leads to the desired representation

$$K_S^{\rm col}(t)/3 = D_0^S\,\delta(t) - D_0^{S\,2} F^{\rm col}(t), \tag{A9}$$

where $F^{\rm col}(t)$ obeys Eqs. (23).

Let us add that the backtransformation of Eq. (A8b) leads to an equation of motion determining $F^{\rm col}(t)$ from the kernel $m_S^{\rm col}(t)$:

$$F^{\rm col}(t) = m_S^{\rm col}(t) - D_0^S \int_0^t dt'\, m_S^{\rm col}(t-t')\, F^{\rm col}(t'). \tag{A10}$$

Integrating Eq. (A9) twice with respect to the time and using Eq. (A10), one gets an equation of motion for the MSD of the colloid,

$$\Delta_S^{\rm col}(t) = D_0^S\left[t - \int_0^t dt'\, m_S^{\rm col}(t-t')\, \Delta_S^{\rm col}(t') \right]. \tag{A11}$$

This result was derived originally along a different route [23]. It implies $\lim_{t\to 0}\Delta_S^{\rm col}(t)/t = D_0^S$.

[1] J.-P. Hansen and I. R. McDonald, *Theory of Simple Liquids*, 2nd ed. (Academic Press, London, 1986).
[2] W. van Megen, T. C. Mortensen, S. R. Williams, and J. Müller, Phys. Rev. E **58**, 6073 (1998).
[3] W. K. Kegel and A. van Blaaderen, Science **287**, 290 (2000).
[4] E. R. Weeks, J. C. Crocker, A. C. Levitt, A. Schofield, and D. A. Weitz, Science **287**, 627 (2000).
[5] W. Kob and H. C. Andersen, Phys. Rev. E **51**, 4626 (1995).
[6] S. Kämmerer, W. Kob, and R. Schilling, Phys. Rev. E **58**, 2131 (1998).
[7] S. R. Kudchadkar and J. M. Wiest, J. Chem. Phys. **103**, 8566 (1995).
[8] S. Mossa, R. Di Leonardo, G. Ruocco, and M. Sampoli, Phys. Rev. E **62**, 612 (2000).
[9] P. Gallo, F. Sciortino, P. Tartaglia, and S.-H. Chen, Phys. Rev. Lett. **76**, 2730 (1996).
[10] B. Doliwa and A. Heuer, J. Phys.: Condens. Matter **11**, A277 (1999).
[11] J. Horbach and W. Kob, Phys. Rev. B **60**, 3169 (1999).
[12] W. Götze, in *Liquids, Freezing and Glass Transition*, edited by J.-P. Hansen, D. Levesque, and J. Zinn-Justin (North-Holland, Amsterdam, 1991), p. 287.
[13] R. Schilling, in *Disorder Effects on Relaxational Processes*, edited by R. Richert and A. Blumen (Springer-Verlag, Berlin, 1994), p. 193.
[14] W. Götze, J. Phys.: Condens. Matter **11**, A1 (1999).
[15] J. Wuttke, M. Ohl, M. Goldammer, S. Roth, U. Schneider, P. Lunkenheimer, R. Kahn, B. Rufflé, R. Lechner, and M. A. Berg, Phys. Rev. E **61**, 2730 (2000).
[16] R. Torre, P. Bartolini, M. Ricci, and R. M. Pick, Europhys. Lett. **52**, 324 (2000).
[17] G. Hinze, D. D. Brace, S. D. Gottke, and M. D. Fayer, J. Chem. Phys. **113**, 3723 (2000).
[18] T. Gleim and W. Kob, Eur. Phys. J. B **13**, 83 (2000).
[19] F. Sciortino and W. Kob, Phys. Rev. Lett. **86**, 648 (2001).
[20] M. Fuchs, I. Hofacker, and A. Latz, Phys. Rev. A **45**, 898 (1992).
[21] M. Fuchs, Transp. Theory Stat. Phys. **24**, 855 (1995).
[22] T. Franosch, M. Fuchs, W. Götze, M. R. Mayr, and A. P. Singh, Phys. Rev. E **55**, 7153 (1997).
[23] M. Fuchs, W. Götze, and M. R. Mayr, Phys. Rev. E **58**, 3384 (1998).
[24] W. Götze and M. R. Mayr, Phys. Rev. E **61**, 587 (2000).
[25] S.-H. Chong, W. Götze, and A. P. Singh, Phys. Rev. E **63**, 011 206 (2001).
[26] D. Chandler and H. C. Andersen, J. Chem. Phys. **57**, 1930 (1972).
[27] U. Bengtzelius, W. Götze, and A. Sjölander, J. Phys. C **17**, 5915 (1984).
[28] T. Franosch, W. Götze, M. R. Mayr, and A. P. Singh, J. Non-Cryst. Solids **235-237**, 71 (1998).
[29] T. Franosch and A. P. Singh, J. Chem. Phys. **107**, 5524 (1997).
[30] W. Götze and L. Sjögren, Rep. Prog. Phys. **55**, 241 (1992).
[31] M. Fuchs and Th. Voigtmann, Philos. Mag. B **79**, 1799 (1999).
[32] W. Götze and L. Sjögren, J. Math. Anal. Appl. **195**, 230 (1995).
[33] G. Gripenberg, S. O. Londen, and O. Staffans, *Volterra Integral and Functional Equations*, Vol. 34 of *Encyclopedia of Mathematics and Its Applications* (Cambridge University Press, Cambridge, 1990).
[34] T. Franosch and W. Götze, J. Phys. Chem. B **103**, 4011 (1999).
[35] W. Götze, A. P. Singh, and Th Voigtmann, Phys. Rev. E **61**, 6934 (2000).
[36] C. Bennemann, J. Baschnagel, W. Paul, and K. Binder, Comput. Theor. Polym. Sci. **9**, 217 (1999).
[37] C. Donati, J. F. Douglas, W. Kob, S. J. Plimpton, P. H. Poole, and S. C. Glotzer, Phys. Rev. Lett. **80**, 2338 (1998).